frontiers in Materials

ORIGINAL RESEARCH
published: 05 January 2022
doi: 10.3389/fmats.2021.804328

Active Corrosion Protection by Epoxy Coating on Li_2CO_3-Pretreated Anodized Aluminum Alloy 2024-T3

Badar Minhas, Sahib Dino, Luyao Huang and Dequan Wu*

Institute for Advanced Materials and Technology, University of Science and Technology Beijing, Beijing, China

The fast leaching and robust barrier property of inhibitors are the basic fundamentals for the formation of active protective coatings to protect aluminum alloys. Herein, an active protective surface was developed based on an epoxy coating and an underlying lithium carbonate (Li_2CO_3)-treated anodized aluminum alloy 2024-T3. The morphology of the Li-LDH layer was studied to know its formation mechanism. The electrochemical studies revealed that the fast and adequate leaching of lithium led to a substantial increment of corrosion resistance of the scratched coating in 3.5 wt% NaCl from 1 to 8 days. Time of flight secondary ion mass spectroscopy (ToF-SIMS) results indicated that Li was distributed in the lateral direction and covered the scratched area. The 3D images indicated that different lithium compounds were formed and 90% of the scratched area was covered with the lithium protective layer over immersion time. A combined approach of morphology observations, electrochemical measurements, and ToF-SIMS showed the lithium protective layer offered good corrosion resistance. On the contrary, lithium provided fast and adequate leaching from the coating, demonstrating good active protection for aluminum and its alloys.

Keywords: lithium inhibitors, aluminum alloy 2024-T3, coating, ToF-SIMS, corrosion protection

OPEN ACCESS

Edited by:
Xiaoqiang Fan,
Southwest Jiaotong University, China

Reviewed by:
Mahmood Aliofkhazraei,
Tarbiat Modares University, Iran
Han Yan,
Southwest Jiaotong University, China

****Correspondence:***
Badar Minhas
badar.minhas@outlook.com

Specialty section:
This article was submitted to Environmental Degradation of Materials, a section of the journal Frontiers in Materials

Received: *29 October 2021*
Accepted: *07 December 2021*
Published: *05 January 2022*

Citation:
Minhas B, Dino S, Huang L and Wu D (2022) Active Corrosion Protection by Epoxy Coating on Li_2CO_3-Pretreated Anodized Aluminum Alloy 2024-T3. Front. Mater. 8:804328. doi: 10.3389/fmats.2021.804328

INTRODUCTION

In the aerospace industries, the corrosion protection of aluminum alloys is of great significance (Buchheit et al., 1993; Kendig and Buchheit, 2003; Visser et al., 2018a), which is principally achieved by anodic oxidation incorporated with the Cr(VI) conversion process. However, this approach will be banned by regulatory authorities in the near future due to the hazardous and carcinogenic effects of chromate commercial coatings. 2024-T3 aluminum alloy, one of the most commonly used aluminum alloys, is prone to localized corrosion in the chloride-containing medium due to the presence of intermetallic particles (IMPs). The IMPs provide active sites for corrosion initiation and propagation with respect to the surrounding matrix (Yasakau et al., 2006). Kosari et al. (2020) and Kosari et al. (2021a) studied the initiation, propagation, and dealloying of IMPs in 0.01 M NaCl solution by liquid phase transmission electron microscopy (LP-TEM). *In situ* TEM images revealed that the main cause of corrosion initiation to the propagation of aluminum alloy was the S-phase (Al_2CuMg) and θ-phase (Al_2Cu). The S-phase was more electrochemically active than the θ-phase and showed fast local degradation upon exposure to corrosive media. Over time, different IMPs cause local corrosion on an aluminum alloy such as pitting, intergranular corrosion, and copper redistribution process. To eradicate the electrochemical reactions on IMPs, it is urgent to design eco-friendly, highly protective, and cost-effective coatings to replace chromate-based surface technologies.

In recent years, many breakthroughs related to Cr(VI)-free coatings have been reported, particularly for corrosion protection of 2024-T3 aluminum alloys. In particular, the active protective coatings possessing both the barrier property from the coating matrix and the inhibition effect from the incorporated corrosion inhibitors are shown to be more promising for corrosion protection than the regular barrier-type coatings (Zhang et al., 2018; Ma et al., 2021a; Ma et al., 2021b). In case of mechanical damages on the coating surface, the incorporated inhibitors in the coating will leach out and protect the damaged coating area. Lithium salts have been demonstrated to be excellent corrosion inhibitors toward aluminum and its alloys for active protection. For example, Drewien et al. (1996) introduced a lithium-based conversion layer by exposing the 1,100 aluminum alloy in Li_2CO_3 solution at different pH values. Visser et al. (2016), Visser et al. (2017), Visser et al. (2018a), Visser et al. (2018b), and Visser et al. (2019a) found another way of utilizing lithium inhibitors by adding them directly into the epoxy coating which was applied on the aluminum alloy surface. The lithium salts mixed in the coating could leach out under aggressive environments and establish an alkaline condition that enabled the generation of a protective film on the defective area in the coating, therefore successfully stifling the electrochemical process. In addition, a recent work of Visser et al. (2019b) demonstrated that lithium salt incorporated in an organic coating could leach out with high chemical throwing power over a broad width of an artificial coating defect. Kosari et al. (2021b) and Bouali et al. (2021) developed a lithium-based double hydroxide (LDH) layer on the aluminum alloy surface, and demonstrated that the immersion in alkaline solution induced the surface enrichment of Cu which favored the growth of the Li-LDH layer *via* aluminum and magnesium dissolution. Andressa et al. (Trentin et al., 2019) observed the effect of lithium on poly (methyl methacrylate) (PMMA) silica sol–gel coating. The addition of lithium resulted in a densified network of PMMA by reduction in the stacking defect and provided active protection as restoration of the system over a long immersion time. Many researchers performed the plasma electrolytic oxidation (PEO) and micro arc oxidation (MAO) on Mg and Al alloys to obtain the porous structure that solved the relative adhesion problems of polymer top coatings on the surfaces. Furthermore, the PEO and MAO surfaces acted as containers to store different inhibitors, and the pH changes provided active corrosion protection in the defect area and improved its barrier properties (Golabadi et al., 2017a; Yang et al., 2018a; Yang et al., 2018b; Pezzato et al., 2019; Toorani and Aliofkhazraei, 2019; Toorani et al., 2019; Toorani et al., 2020; Liu et al., 2021; Ostapiuk, 2021; Toorani et al., 2021; Zeng et al., 2021; Zhang et al., 2021). Golabadi et al. (2017b) showed that the compaction and cathodic disbondment of the epoxy coating were enhanced on the phosphated coating consisting of different additives.

In the present work, a new active protective coating was designed on the 2024-T3 aluminum alloy surface to protect it against localized corrosion. A concave anodic aluminum oxide (AAO) layer was first formed on the 2024-T3 aluminum alloy and was immersed in lithium carbonate solution to obtain a lithium-based protective layer (Li-AAO). To explore the active protective response, an epoxy coating was further applied onto Li-AAO and was scratched before immersion in a 3.5 wt% NaCl solution. The formation and growth mechanism of the lithium-based protective layer on aluminum alloy were studied by various analytical techniques including scanning electron microscopy (SEM), transmission electron microscopy (TEM), and time-of-flight–secondary ion mass spectroscopy (ToF-SIMS). The corrosion resistance property of the generated layers was investigated using electrochemical impedance spectroscopy (EIS) and potentiodynamic polarization.

EXPERIMENTAL SECTION

Materials and Coating Preparation

As received, aluminum alloy sheets 2024-T3 [12.7 cm (L) × 7.6 cm (W)] formed by cutting were used as the substrates. In order to introduce the concave AAO surfaces, an electrochemical polishing pretreatment was applied on the aluminum alloy prior to anodization (Montero-Moreno et al., 2007). First, electrochemical polishing was conducted at 20 V (vs. calomel reference electrode) in a potentiostatic mode at 0–5°C, in a mixture of ethanol (900 ml), perchloric acid (80 ml), and distilled water (20 ml), under continuous stirring for 1 min. Afterward, the substrate was etched in 10 wt% NaOH alkaline solution for 5 min at 55°C, followed by desmutting in 30 vol% HNO_3 at ambient temperature. The aforementioned steps were repeated once, followed by etching in a mixture of 6 wt% H_3PO_4 and 1.8 wt% CrO_3 for 1 min at 55°C. The polished substrates were thoroughly rinsed with distilled water for 2 min. Thereafter, a two-step anodization process was used (Zaraska et al., 2010; Elaish et al., 2018). The pretreated samples were anodized in an electrochemical cell at 32 V (vs. saturated calomel electrode) in 0.3 M H_2SO_4 for 1 h, with aluminum alloy as the anode and graphite as the cathode. The bath temperature was maintained at 0–5°C under continuous stirring. The first concave layer formed after anodization was removed by acid etching in the mixture of 6 wt% H_3PO_4 and 1.8 wt% CrO_3 for 5 min at 45°C. The second anodization was performed under the same condition. Finally, the samples were rinsed with distilled water and air-dried at room temperature.

In order to prepare the lithium-based protective coatings, the anodized aluminum surface was immersed in 0.1 M Li_2CO_3 solution at 25°C for 24 h. The Li-based film was formed by a coprecipitation reaction involving Al; therefore, a sacrificial aluminum substrate was also immersed in the solution and allowed to dissolve freely. The pH of the solution was controlled to be 11.5 during the reaction. Thereafter, the samples were taken out and air-dried, which were named Li-AAO substrate. The Li-AAO substrates were further coated with an epoxy coating and cured at 55°C for 24 h (denoted as Li-AAO/epoxy coating). The epoxy coating was applied with a bar coater to control a final thickness of ~25 μm (Visser et al., 2017). An artificially scratched area (1–1.5 mm in width) was made by a surgical knife on the Li-AAO epoxy coating surface before immersion in 3.5 wt% NaCl solution. For comparison, an AAO substrate without lithium inhibitor

treatment was also coated with an epoxy coating and named AAO/epoxy coating.

Electrochemical Measurements

The EIS measurements of the 1) AAO substrate, 2) Li-AAO substrate, 3) scratched AAO/epoxy coating, and 4) scratched Li-AAO/epoxy coating were conducted using Princeton applied research PARSTAT 2273 potentiostat after immersion in 3.5 wt% NaCl solution for 1, 3, 5, and 8 days. A classic three-electrode electrochemical cell was used, with the (coated) aluminum substrate as the working electrode, a platinum foil as the counter electrode, and a saturated calomel electrode (SCE) as the reference electrode (Visser et al., 2018a). EIS tests were executed in a frequency range 10^{-2}–10^{5} Hz with a perturbation of 10 mV. EIS data were fitted using suitable equivalent electric circuits (EECs) by ZSimpWin software. To ensure reproducibility, each measurement was repeated at least three times. Potentiodynamic polarizations were performed on the samples after 8 days of immersion in 3.5 wt% NaCl solution, with a scan rate of 1 mV/s.

Surface Analytical Measurements

The top and cross-sectional images of the AAO substrate and Li-AAO substrate were obtained by SEM (SU8200 Hitachi, Japan). The cross section of the Li-AAO substrate was prepared using focused ion beam (FIB) of Ga^{+} ion Zeiss Auriga Compact Cross Beam SEM (ZEISS 540) and was characterized by TEM observation (TALOS F200X).

ToF-SIMS Measurement

ToF-SIMS measurements were carried out using ToF-SIMS GmbH (ION-TOF, Germany), equipped with a 30 keV Bi^{+} primary ion beam source worked in a high-current mode to obtain the high-resolution mass spectra. Positive mass spectra were obtained over a mass range of 1–800 amu and computed with the known fragments. The exact mass of the fragments was measured (in ppm) by the absolute difference between the experimental and theoretical mass, and the obtained result was divided by experimental mass. The lithium-layered double hydroxide (Li-LDH), lithium with pseudoboehmite (Li-PB), and pseudoboehmite (PB) were acquired by rastering area in patches of 300 μm × 300 μm from the large image area. The analysis for each patch was done for 60 s at a pixel density of 250 pixel/mm. According to the method reported by Marcoen et al. (2018), a peak list with high-resolution spectra was established for the reference sample and finally applied to the attained spectra.

The ToF-SIMS data were analyzed by simsMVA software, and 3D images were produced by Epina Image lab software (Shi et al., 2020). Two functions were used in simsMVA. The first one was the normalization and Poisson scaling of all peak intensities based on the method reported in the literature (Trindade et al., 2018). The second one was the non-negative matrix factorization (NMF), which was used to identify the distribution and presence of pure compounds on the surface.

Reference materials were made for the composition analysis of the lithium protective layer in the scratched area. Specifically, aluminum alloy substrates were thoroughly cleaned and coated with epoxy coating. PB and Li–PB reference samples were prepared according to the method reported by Gorman et al. (2003). The samples were scratched and then exposed to the (i) deionized water or (ii) a 0.02 M LiCl solution at 95–100°C to acquire PB or Li–PB, respectively. The reference of the Al–Li LDH layer is prepared by following the work of Drewien et al. (1996). According to this method, the AA-2024T3 substrates were immersed in 0.1 M Li_2CO_3 solution for 15 min. Finally, the treated substrate was washed thoroughly with deionized water and air-dried at room temperature. All ToF-SIMS measurements were performed in the scratched area.

RESULTS AND DISCUSSION

Figure 1A shows the concaved AAO surface formed on the aluminum alloy 2024-T3 substrate. Unlike the hexagonal array of AAO on pure aluminum (Wu et al., 2019; Wu et al., 2021), the uneven morphology of the nanopores on the AAO surface obtained in this study can be attributed to the potential difference between IMPs and the alloy matrix (Abrahami et al., 2017). **Figures 1B,C** are the top and cross-sectional views of the AAO surface treated with Li_2CO_3 inhibitors (Li-AAO substrate), presenting a plate-like LDH layer with somewhat irregular spacing (Visser et al., 2016). This LDH layer is formed due to the intercalation of lithium into the aluminum hydroxide gel. The AAO and Li-AAO substrates were then cured at 55°C for 24 h to simulate their changes during the curing process when epoxy coating was applied. **Figures 1D,E** are the top and cross-sectional SEM images of the Li-AAO substrate cured at 55°C. **Figure 1D** shows that the LDH layer became smaller flakes after curing. From the cross-sectional image (**Figures 1E,F**), the Li-AAO substrate displayed three defined regions including the columnar, the porous, and the barrier layers from the top to the bottom (Visser et al., 2018a).

EIS Measurements

EIS measurements were conducted on the samples with and without lithium inhibitors, followed by epoxy top coating during the 8 days of immersion in a 3.5% NaCl solution (**Figure 2**). **Figures 2A–C** show the Nyquist and Bode plots of the uncoated AAO surfaces without lithium inhibitors. The semi-capacitive arcs in Nyquist plots become smaller due to pitting corrosion with the prolonging of immersion time. The low-frequency impedance value at 10^{-2} Hz ($|Z|_{0.01Hz}$), which is a common indicator of the corrosion resistance (Buchheit et al., 1993), decreased slightly from 16.2 kΩ cm^2 (1 day) to 11.5 kΩ cm^2 (8 days). In the phase plots of **Figure 2C**, two time constants were shown; the one at low frequency (10^{-2}–10^{-1} Hz) was related to the electrochemical activity on the aluminum alloy surface, and the second one at middle frequency (10^{1}–10^{3} Hz) was ascribed to the oxide layer (Visser et al., 2017). It was shown in **Figure 2C** that the active corrosion was observed as the immersion time increased on the uncoated AAO surface. The EIS spectra of the Li-AAO substrate are shown in **Figures 2D–F**. The capacitive arcs remained almost unchanged over 8 days, denoting that the lithium protective

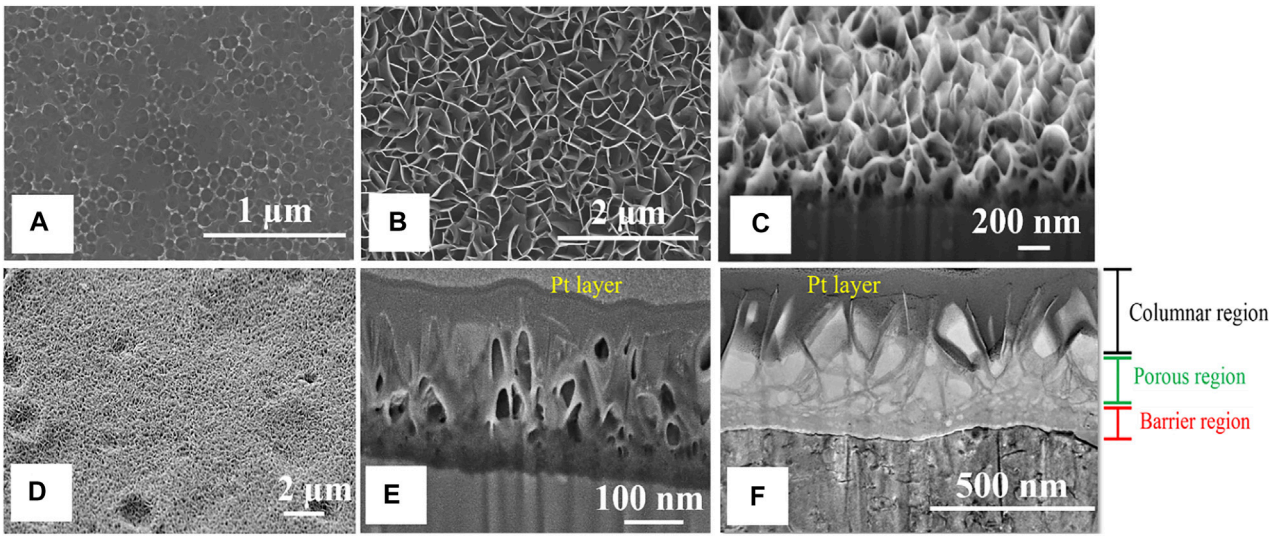

FIGURE 1 | SEM images of **(A)** the top view AAO surface on 2024-T3 substrate, **(B)** top view, and **(C)** cross-sectional view of the Li-AAO substrate; SEM images of **(D)** top view and **(E)** cross-sectional view of the Li-AAO substrate after curing at 55°C; **(F)** TEM image of the cross-sectional view of the Li-AAO substrate after curing at 55°C.

layer showed high interfacial resistance to the corrosion process (Visser et al., 2018a). In the Bode impedance plots, the $|Z|_{0.01Hz}$ values slightly increased from 1.0 MΩ cm^2 (day 1) to 1.3 MΩ (day 8). From the phase angle plots, three time constants were observed; the one at the low-frequency region (10^{-2}–10^{-1} Hz) represented corrosion on the metal surface, and the other two time constants overlapped in the broad middle frequency range and were attributed to the dense and porous regions of the lithium protective layer (Liu et al., 2016). The EIS spectra of Li-AAO illustrated that the lithium protective layer showed a significant corrosion protection as compared to the uncoated AAO substrate. The EIS spectra of the scratched AAO/epoxy coating are illustrated in **Figures 2G–I**. The Nyquist plots showed a decrease in size of the capacitive arcs after 1 day. In the Bode impedance plots, the $|Z|_{0.01Hz}$ displayed a small change within 8 days. The Nyquist and Bode plots of scratched Li-AAO/epoxy coating are presented in **Figures 2J–L**. The obvious increase in the size of capacitive arcs signified the growth of the protective layer in the scratched area. From the Bode impedance plots, the $|Z|_{0.01Hz}$ value changed from 0.6 MΩ cm^2 (1 day) to 2.2 MΩ cm^2 (8 days), determining that the corrosion protection property was improved. From the Bode phase plots, three time constants were observed. The time constant at low frequency (10^{-2} Hz) at day 1 was ascribed to the electrochemical activity. The second and third time constants were noticed at the middle frequency region (10^{1}–10^{3} Hz), which were referred to the dense and porous regions of the lithium protective layer (Visser et al., 2018a; Trentin et al., 2019). The time constant at the low frequency disappeared after 1 day of immersion. It should be noted the EIS spectra of Li-AAO in **Figures 2D–F** present slightly different results compared with those of the scratched Li-AAO/epoxy coating (**Figures 2J–L**). The main reason is associated with the lithium leaches from the complex network of the columnar region into the scratched area that further densified the porous and barrier regions next to the substrate. In contrast, the Li-AAO substrate shows the EIS measurements from the top surface with no scratched area. As a result, the corrosion protection of the scratched Li-AAO/epoxy coating was increased over time (Kosari et al., 2021b). The EIS spectra of scratched Li-AAO/epoxy coating showed that lithium leached from the lithium protective layer and provided active protection in the scratched area over the immersion time. Diping and their coworkers performed plasma electrolytic oxidation (PEO) on UNS A97075 Al alloy and further sealed this layer with silane. The corrosion property of PEO sealed with silane was measured by electrochemical impedance spectroscopy (EIS). The measured corrosion resistance of aluminum alloy was good but lower than that of the present study (Zeng et al., 2021).

The EIS measurements were fitted by the EECs in **Figure 3** to evaluate the electrochemical response of different substrates. **Figure 3A** displays an EEC with two time constants, which is used to describe the electrochemical response in the damaged area without the lithium inhibitors. In this circuit, R_{sol} describes the solution resistance; R_{oxide} and CPE_{oxide} represent the resistance and capacitance of the AAO layer; and R_{ct} and CPE_{dl} depict the electrochemical responses at the aluminum alloy surface *via* charge transfer resistance and double layer capacitance, respectively (Visser et al., 2018a; Visser et al., 2017). Generally, CPE is used instead of a pure capacitance to define the non-ideal capacitive behavior of elements, which is mainly attributed to the uneven growth of the generated layer (Hsu and Mansfeld, 2001). An EEC with three time constants in **Figure 3B** is used to fit the EIS data of AAO with lithium inhibitors. In this model, an additional time constant is contributed to the generated lithium-based protective layer, which is in good agreement with the SEM and TEM results in

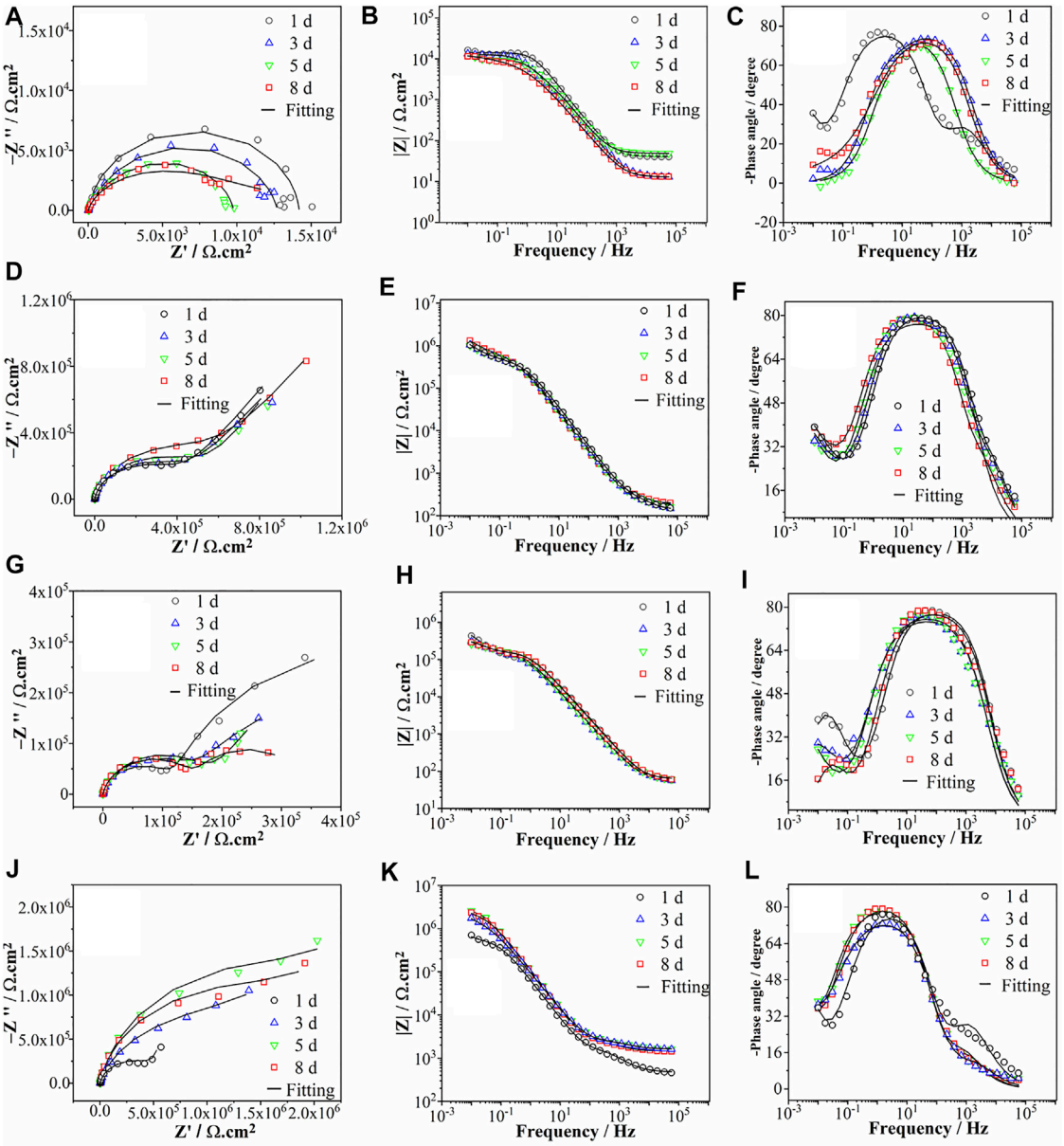

FIGURE 2 | EIS spectra of the **(A–C)** AAO substrate, **(D–F)** Li-AAO substrate, **(G–I)** scratched AAO/epoxy coating, and **(J–L)** scratched Li-AAO/epoxy coating during immersion in 3.5% NaCl solution from 1 to 8 days.

Figures 1E,F. R_{sol} describes the solution resistance, R_{porous} and CPE_{porous} represent the resistance and capacitance of the porous layer, respectively, and R_{oxide} and CPE_{oxide} refer to the capacitance and resistance of the combination of the AAO layer and dense layer, respectively. **Figure 3B** shows that an additional time constant attributed to the porous oxide layer formed on the barrier layer. The equivalent capacitance values of different elements in **Figures 3A,B** can be calculated by using CPE values (Q and n) with their respective resistance according to the following **Eq. 1** (Golabadi et al., 2017b).

$$C = Q^{1/n} R^{(1-n)/n}. \quad (1)$$

Figure 4A illustrates the variation of R_{oxide} with respect to the immersion time. For the AAO substrate, the R_{oxide} value was as low as ~100 kΩ cm^{-2} at the beginning of immersion (1 day), whereas the R_{oxide} value of the Li-AAO substrate was relatively high (2590 kΩ cm^{-2}) after 1 day. After application of the epoxy coating, the R_{oxide} of the scratched AAO/epoxy coating remained as low as ~463 kΩ cm^{-2} during the 8 days of immersion. The R_{oxide} of the scratched Li-AAO/epoxy coating was ~2500 kΩ cm^{-2} after 1 day, which increased to ~7,500 kΩ cm^{-2} after 5 days, and then decreased to 4,300 kΩ cm^{-2} after 8 days. The corresponding CPE_{oxide} values of different coatings are shown in **Figure 4B**. The CPE_{oxide} of the

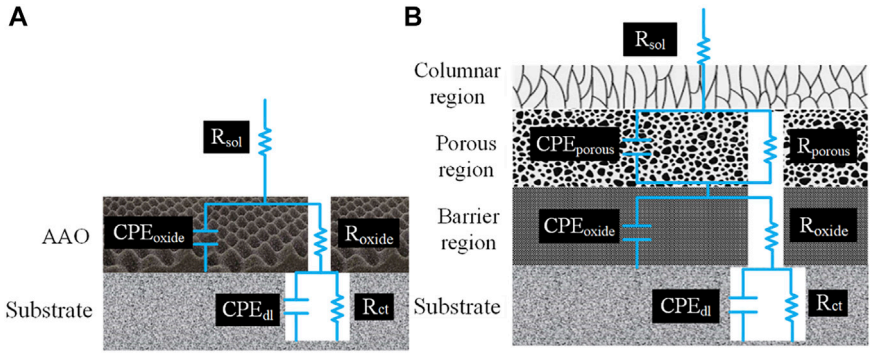

FIGURE 3 | Equivalent electric circuits used to fit EIS spectra **(A)** without inhibitors and **(B)** with inhibitors.

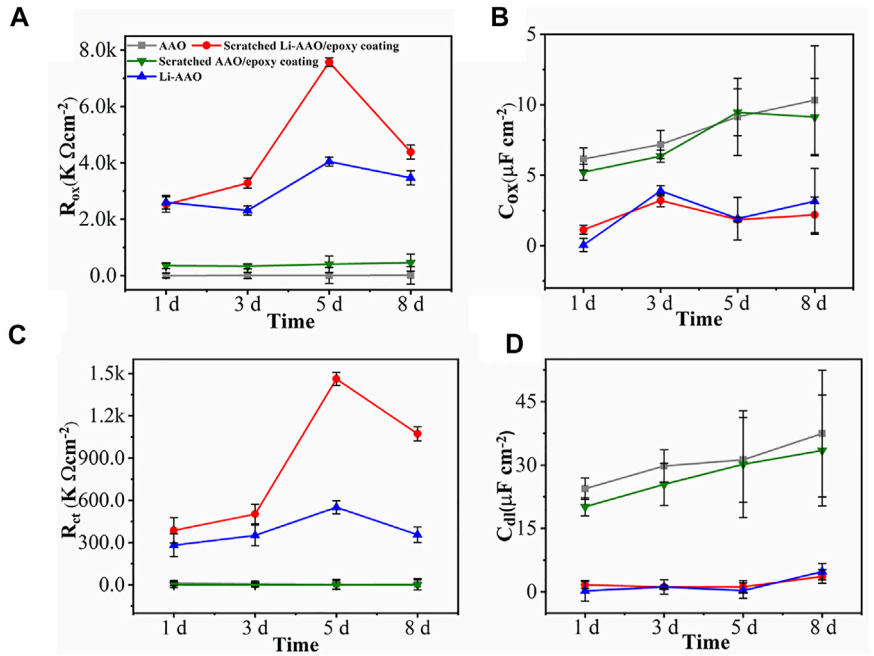

FIGURE 4 | Evolution of the **(A)** oxide resistance (R_{oxide}), **(B)** oxide capacitance (C_{oxide}), **(C)** charge transfer resistance (R_{ct}), and **(D)** double-layer capacitance (C_{dl}) of the AAO substrate, Li-AAO substrate, scratched AAO/epoxy coating, and scratched Li-AAO/epoxy coating.

AAO substrate and scratched AAO/epoxy coating showed an increase over time. The CPE_{oxide} values of the Li-AAO substrate and the scratched Li-AAO/epoxy coating were much lower, and a slight increase in the CPE_{oxide} was observed after 1 day, which was attributed to the development of the lithium-based protective layer. The corrosion rate of the surfaces can be estimated by R_{ct} values, which are shown in **Figure 4C**. The R_{ct} of samples without inhibitors showed much lower values throughout the entire immersion. R_{ct} was higher in case of the Li-AAO substrate, which was ~267 kΩ cm^{-2} after 1 day, and increased to ~552 kΩ cm^{-2} after 5 days, and then decreased to 363 kΩ cm^{-2} after 8 days. The R_{ct} of the scratched Li-AAO/epoxy coating was the highest, being 389 kΩ cm^{-2} after 1 day, and increased up to ~1,469 kΩ cm^{-2} after 5 days, and then slightly decreased to 1,075 kΩ cm^{-2} after 8 days. In **Figure 4D**, the variation of the CPE_{dl} values is in good agreement with that of the R_{ct} values for all samples. The samples containing Li inhibitors possess higher resistance values and smaller CPE values, demonstrating a better corrosion protection property. The active protection by the lithium protective layer was determined by the R_{oxide} and R_{ct} values. Comparing Li-AAOs with the uncoated AAO and scratched AAO/epoxy coating, the R_{oxide} and R_{ct} values showed a remarkable increment. A similar trend was observed in the CPE_{oxide} and C_{dl} values as compared to the oxide resistance (R_{oxide}) and charge transfer resistance (R_{ct}) values. The higher R_{ct} values of Li-AAOs after 1 day displayed that the lithium

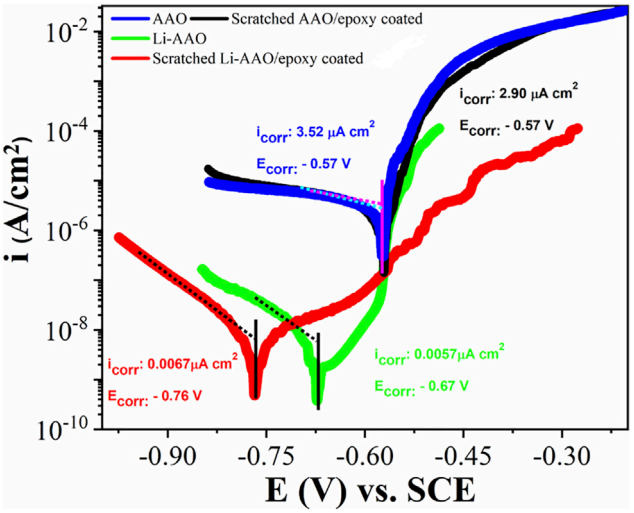

FIGURE 5 | Potentiodynamic polarization curves of the AAO substrate, Li-AAO substrate, scratched AAO/epoxy coating, and scratched Li-AAO/epoxy coating.

protective layer showed good barrier properties. Further increment in R_{ct} values from 3 to 8 days ascribed the lithium leaching from the lithium layer, providing active protection in the scratched area. Toorani et al. (2019) performed micro arc oxidation on AZ31-magnesium alloy, and the existing porous structure was closed by cerium oxide and was epoxy-coated further. The different nominal concentration of cerium oxide was used, and the corrosion property was observed at the defined scratched zone. The layer exhibited good corrosion protection and was much comparable with the present study (Toorani and Aliofkhazraei, 2019).

Potentiodynamic Polarization Measurements

Figure 5 shows the polarization measurements of the AAO substrate, Li-AAO substrate, scratched AAO/epoxy coating, and scratched Li-AAO/epoxy coating after 8 days of immersion in 3.5% NaCl solution. The curves of the AAO substrate and the scratched AAO/epoxy coating overlapped with each other. Both curves showed active corrosion during anodic polarization with respect to the open circuit potential (OCP). The cathodic branches exhibited higher current densities than the Li-AAO substrate, which were ascribed to the diffusion-limited reduction of dissolved oxygen (Visser et al., 2016; Visser et al., 2018a). In contrast, the Li-AAO substrate showed effective corrosion inhibition after 8 days of immersion. The anodic polarization of the Li-AAO substrate showed a small passive range from −670 to −570 mV. Unlike the Li-AAO substrate, the scratched Li-AAO/epoxy coating after 8 days of immersion in 3.5% NaCl solution showed passivation behavior in the anodic region (Visser et al., 2017). The anodic polarization exhibited the anodic passive range, with no sign of pitting corrosion as compared to the Li-AAO substrate. The cathodic branches of Li-AAOs showed lower current density, indicating the oxygen reduction reaction is suppressed. This shows that the cathodic inhibition of Li-AAOs is due to the leaching of lithium from the lithium protective layer. The corrosion current (i_{corr}) is measured by extrapolating the cathodic branch that has a linear Tafel region to intersect with OCP. By analyzing the electrochemical parameters in **Figure 5**, it can be deduced that the Li-AAO samples yield a corrosion inhibition effect as compared to the samples without inhibitors.

Li Distribution and Composition Tested by ToF-SIMS

Li is a low atomic number element that is very difficult to be detected using the typical surface analytical approaches (Marcoen et al., 2018). ToF-SIMS with high sensitivity to the lithium element was hence proposed to analyze the distribution and composition of the generated protective layer on AA2024-T3. ToF-SIMS measurements are performed in the scratched area with the omission of areas near the edges to eradicate the artefacts. A multivariant analysis method, that is, non-negative matrix factorization (NMF), was used to figure out the various elements present on the protective surface. The NMF function was applied to know the relative chemical composition of Li species after leaching in the scratched area with respect to the reference material. Three reference materials (Li-LDH, Li–PB, and PB)

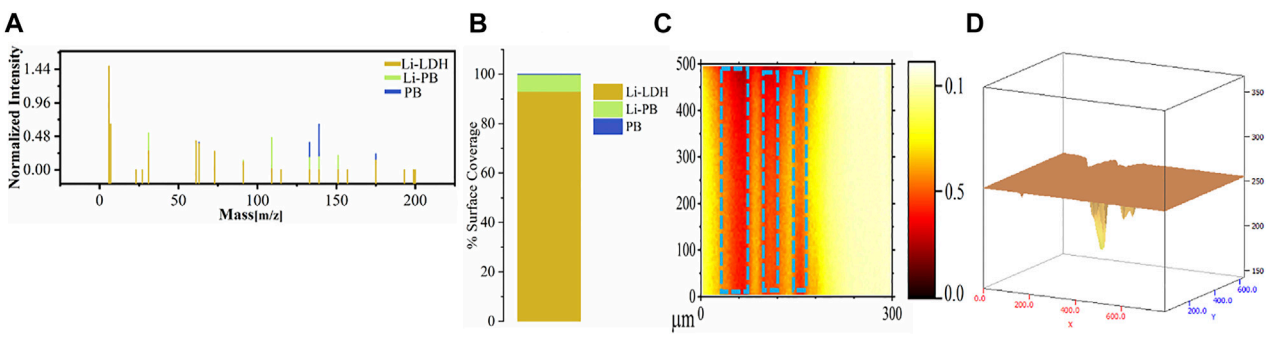

FIGURE 6 | Reference material data for ToF-SIMS analysis: **(A)** mass spectrum, **(B)** surface coverage, **(C)** ToF-SIMS, and **(D)** 3D image.

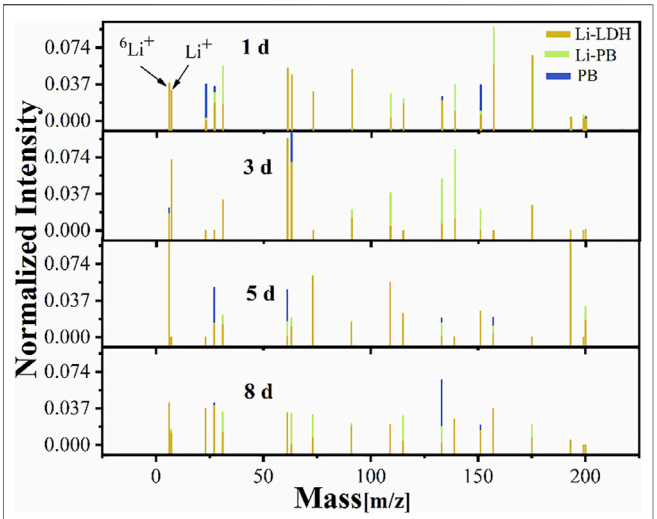

FIGURE 7 | Positive ToF-SIMS mass spectra data from PB, Li–PB, and Li-LDH; the mass spectra are normalized to the total ion intensity.

were prepared, and their respective data are shown in **Figures 6A–D** (Yang et al., 2018a; Visser et al., 2019b).

Figure 7 shows the NMF mapping of all spectra within 8 days of immersion and was produced by applying the method of Trindade et al. (2018). These maps showed fast leaching of Li^+ over a long immersion time in the scratched area. The NMF mapping was used to determine three chemical compositions in the scratched area. The major attention in the mass ranges was paid to two peaks located at 6 and 7 (*m/z*), which can be attributed to the minor isotope $^6Li^+$ and Li^+ ion, respectively. The presence of both peaks in each spectrum indicates that lithium was incorporated in the LDH structures. The maps for lithium distribution are monitored by the minor isotope $^6Li^+$ in the scratched area. Li^+ was found to saturate in the detector, and its natural abundance was reported to be 92.5%, and the remaining was minor isotope $^6Li^+$ ion (Marcoen et al., 2018). **Figure 8** discloses that the Li distribution covered the scratched area after 1 day. The inspected scratched areas of 3, 5, and 8 days of coatings revealed different amounts of $^6Li^+$ concentration, suggesting that the surface compositions are different. Furthermore, **Figure 7** shows that the maximum enrichment of Li was seen after 5 days. These results are in good agreement with the EIS data in **Figure 2**.

The 3D images in **Figure 9** show different compound formation in the scratched area over 8 days of immersion. The 3D images showed that different Li-LDH layers were found in the scratched area. The different compounds of lithium were observed due to changes in local pH values in the scratched area, and the leaching of lithium occurred from the lithium protective layer. **Figure 10** illustrates the percentage surface coverage of three different compounds in the scratched area, and the surface coverage data extracted from **Figure 9**. Two or three different regions were seen in the scratched area, indicating that the protective layers were made of different compounds. The formation of the Li-LDH layer depends on the higher pH values, and adequate amounts of $Al(OH)_4^-$, OH^-, CO_3^-, and Li^+ ions should be present in the scratched zone. In

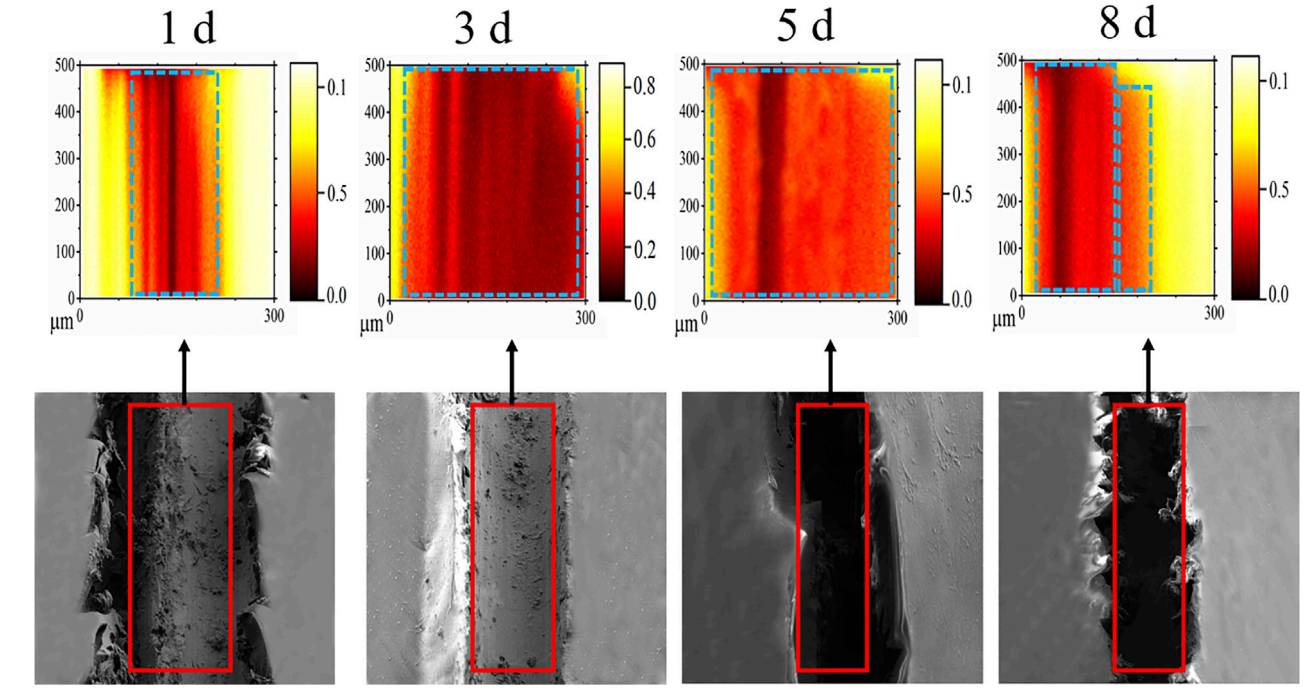

FIGURE 8 | ToF-SIMS and SEM images of the scratched Li-AAO/epoxy coating in the scratched area during immersion in 3.5% NaCl solution from 1 to 8 days; the ToF-SIMS images are normalized to the total ion intensity.

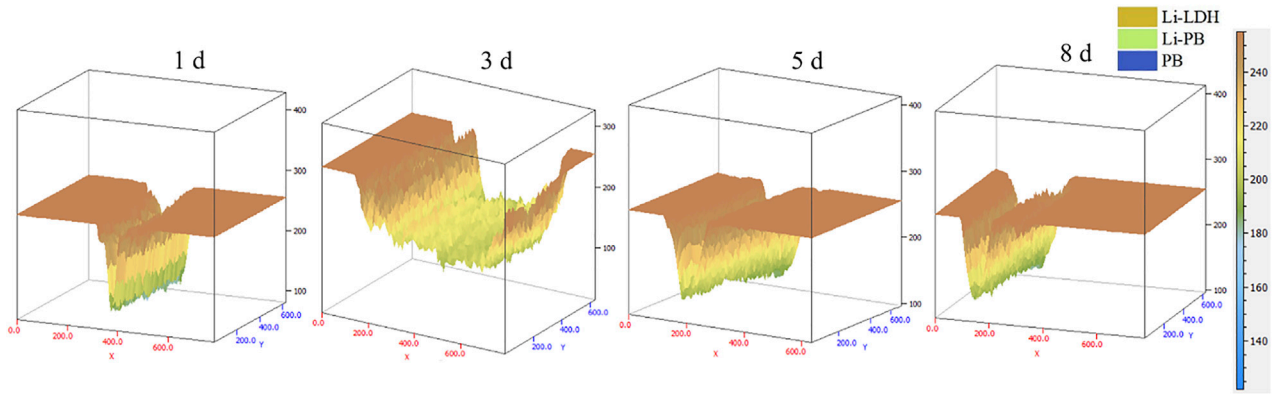

FIGURE 9 | 3D images of PB, Li–PB, and Li-LDH derived from ToF-SIMS data.

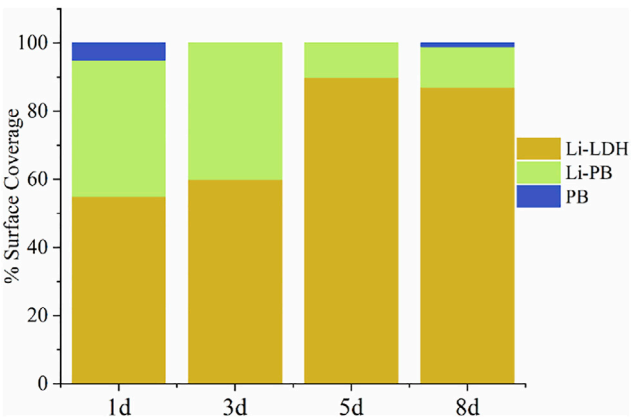

FIGURE 10 | Surface coverage percentage of PB, Li–PB, and Li-LDH derived from 3D images.

Figure 10, 1 and 8 days show three compounds formation, while 3 and 5 days display only two compounds in the scratched area. After 1 day, the leaching of lithium over the immersion time increased, and the main compound that covered the scratched area is Li-LDH. Due to changes in pH values, the Li–PB and PB regions are also observed in the scratched area.

Mechanism of Active Corrosion Inhibition

The mechanism of the lithium protective layer to achieve active corrosion protection in damaged coating can be described as follows based on the EIS, polarization, and ToF-SIMS results. As the scratched Li-AAO/epoxy coating is exposed to the chloride environment, the presence of IMPs on the exposed aluminum alloy substrate such as the S-phase is susceptible to more rapid corrosion. As a result, Al and Mg are dissolved, which leads to Cu enrichment. The oxygen reduction on the Cu develops the alkaline environment that triggers the leaching of lithium from the lithium-based protective layer. Meanwhile, uniform corrosion of Al also occurred, and Al_2O_3 is formed. As the immersion time increased, the continuous increment in the pH value accelerates the lithium leaching rate. It is reported that $Al(OH)_4^-$ was found on the Cu particles at higher pH values, and lithium is easily intercalated into aluminum hydroxide gel (Kosari et al., 2021b; Bouali et al., 2021). Therefore, the Li-LDH layer is observed in high amounts during the 8 days of immersion, gradually covering the scratched area. The pH values in the scratched area are different due to different alloying elements. At mild pH values, a small amount of PB is observed. At higher pH values, Li–PB is also found over the scratched area (Yan et al., 2020). The corrosion process of the scratched Li-AAO/epoxy coating slows down after 1 day, a dense barrier layer (Li-LDH and Li–PB) is formed, and active corrosion protection is thereby achieved as the immersion time prolonged.

CONCLUSION

In this work, a novel active protective surface was developed on anodized 2024-T3 with Li_2CO_3 inhibitors. The growth and barrier property of the lithium protective layer in 3.5 wt% NaCl solution was investigated by SEM and TEM analyses, electrochemical techniques, and ToF-SIMS. The main conclusions of the study are as follows:

1) The active protective coating on 2024-T3 aluminum alloy was formed as a result of precipitation by exposure of anodized 2024-T3 in Li_2CO_3 solution. The formed layer plays a significant role to provide active protection to 2024-T3 aluminum alloy.
2) The EIS results confirmed that the formed layer provided active corrosion protection through the leaching of lithium from the lithium-based layer in the scratched area over the immersion time. The ToF-SIMS analysis provided useful information about the Li distribution in the scratched area.
3) The 3D images of the scratched Li-AAO/epoxy coating showed that the leading compound in the scratched area was Li-LDH, and it can be observed after 1 day of immersion in chloride solution. Another lithium compound, namely, Li–PB, was also observed in the scratched area, and its amount decreased with the immersion time.

DATA AVAILABILITY STATEMENT

The original contributions presented in the study are included in the article/Supplementary Material; further inquiries can be directed to the corresponding author.

AUTHOR CONTRIBUTIONS

BM contributed to supervision, writing—review and editing, conceptualization, investigation, and writing—original draft. SD contributed to conceptualization, investigation, writing—original draft. LH contributed to conceptualization, investigation, and writing—original draft. DW contributed to conceptualization, investigation, material handling, and writing—original draft.

ACKNOWLEDGMENTS

The authors thank Professor Arjan Mol from Delft University of Technology for the helpful discussion.

REFERENCES

Abrahami, S. T., de Kok, J. M. M., Terryn, H., and Mol, J. M. C. (2017). Towards Cr(VI)-free Anodization of Aluminum Alloys for Aerospace Adhesive Bonding Applications: A Review. *Front. Chem. Sci. Eng.* 11, 465–482. doi:10.1007/s11705-017-1641-3

Bouali, A. C., Iuzviuk, M. H., Serdechnova, M., Yasakau, K. A., Drozdenko, D., Lutz, A., et al. (2021). Mechanism of LDH Direct Growth on Aluminum Alloy Surface: A Kinetic and Morphological Approach. *J. Phys. Chem. C* 125, 11687–11701. doi:10.1021/acs.jpcc.1c02281

Buchheit, R. G., Bode, M. D., and Stoner, G. E. (1993). *Talc Coat. Aluminum* 850, 205–214.

Drewien, C. A., Eatough, M. O., Tallant, D. R., Hills, C. R., and Buchheit, R. G. (1996). Lithium-aluminum-carbonate-hydroxide Hydrate Coatings on Aluminum Alloys: Composition, Structure, and Processing bath Chemistry. *J. Mater. Res.* 11, 1507–1513. doi:10.1557/jmr.1996.0188

Elaish, R., Curioni, M., Gowers, K., Kasuga, A., Habazaki, H., Hashimoto, T., et al. (2018). Effect of Fluorozirconic Acid on Anodizing of Aluminium and AA 2024-T3 alloy in Sulphuric and Tartaric-Sulphuric Acids. *Surf. Coat. Technol.* 342, 233–243. doi:10.1016/j.surfcoat.2018.02.096

Golabadi, M., Aliofkhazraei, M., Toorani, M., and Rouhaghdam, A. S. (2017). Evaluation of La Containing PEO Pretreatment on Protective Performance of Epoxy Coating on Magnesium. *Prog. Org. Coat.* 105, 258–266. doi:10.1016/j.porgcoat.2017.01.010

Golabadi, M., Aliofkhazraei, M., Toorani, M., and Sabour Rouhaghdam, A. (2017). Corrosion and Cathodic Disbondment Resistance of Epoxy Coating on Zinc Phosphate Conversion Coating Containing Ni 2+ and Co 2+. *J. Ind. Eng. Chem.* 47, 154–168. doi:10.1016/j.jiec.2016.11.027

Gorman, J. D., Hughes, A. E., Jamieson, D., and Paterson, P. J. K. (2003). Oxide Formation on Aluminium Alloys in Boiling Deionised Water and NaCl, CeCl3 and CrCl3 Solutions. *Corrosion Sci.* 45, 1103–1124. doi:10.1016/s0010-938x(02)00209-3

Hsu, C. H., and Mansfeld, F. (2001). Technical Note: Concerning the Conversion of the Constant Phase Element Parameter Y0 into a Capacitance. *Corrosion* 57, 747–748. doi:10.5006/1.3280607

Kendig, M. W., and Buchheit, R. G. (2003). Corrosion Inhibition of Aluminum and Aluminum Alloys by Soluble Chromates, Chromate Coatings, and Chromate-free Coatings. *Corrosion* 59, 379–400. doi:10.5006/1.3277570

Kosari, A., Ahmadi, M., Tichelaar, F., Visser, P., Gonzalez-Garcia, Y., Zandbergen, H., et al. (2021). Editors' Choice-Dealloying-Driven Cerium Precipitation on Intermetallic Particles in Aerospace Aluminium Alloys. *J. Electrochem. Soc.* 168, 041505. doi:10.1149/1945-7111/abf50d

Kosari, A., Tichelaar, F., Visser, P., Zandbergen, H., Terryn, H., and Mol, J. M. C. (2020). Dealloying-driven Local Corrosion by Intermetallic Constituent Particles and Dispersoids in Aerospace Aluminium Alloys. *Corrosion Sci.* 177, 108947. doi:10.1016/j.corsci.2020.108947

Kosari, A., Tichelaar, F., Visser, P., Zandbergen, H., Terryn, H., and Mol, J. M. C. (2021). Laterally-resolved Formation Mechanism of a Lithium-Based Conversion Layer at the Matrix and Intermetallic Particles in Aerospace Aluminium Alloys. *Corrosion Sci.* 190, 109651. doi:10.1016/j.corsci.2021.109651

Liu, C., Lu, X., Li, Y., Chen, Q., Zhang, T., and Wang, F. (2021). Influence of post-treatment Process on Corrosion and Wear Properties of PEO Coatings on AM50 Mg alloy. *J. Alloys Comp.* 870, 159462. doi:10.1016/j.jallcom.2021.159462

Liu, Y., Visser, P., Zhou, X., Lyon, S. B., Hashimoto, T., Curioni, M., et al. (2016). Protective Film Formation on AA2024-T3 Aluminum Alloy by Leaching of Lithium Carbonate from an Organic Coating. *J. Electrochem. Soc.* 163. C45–C53. doi:10.1149/2.0021603jes

Ma, L., Ren, C., Wang, J., Liu, T., Yang, H., Wang, Y., et al. (2021). Self-reporting Coatings for Autonomous Detection of Coating Damage and Metal Corrosion: A Review. *Chem. Eng. J.* 421, 127854. doi:10.1016/j.cej.2020.127854

Ma, L., Wang, J., Zhang, D., Huang, Y., Huang, L., Wang, P., et al. (2021). Dual-action Self-Healing Protective Coatings with Photothermal Responsive Corrosion Inhibitor Nanocontainers. *Chem. Eng. J.* 404, 127118. doi:10.1016/j.cej.2020.127118

Marcoen, K., Visser, P., Trindade, G. F., Abel, M.-L., Watts, J. F., Mol, J. M. C., et al. (2018). Compositional Study of a Corrosion Protective Layer Formed by Leachable Lithium Salts in a Coating Defect on AA2024-T3 Aluminium Alloys. *Prog. Org. Coat.* 119, 65–75. doi:10.1016/j.porgcoat.2018.02.011

Montero-Moreno, J. M., Sarret, M., and Müller, C. (2007). Influence of the Aluminum Surface on the Final Results of a Two-step Anodizing. *Surf. Coat. Technol.* 201, 6352–6357. doi:10.1016/j.surfcoat.2006.12.003

Ostapiuk, M. (2021). Corrosion Resistance of PEO and Primer Coatings on Magnesium alloy. *J. Asian Ceram. Soc.* 9, 17–29. doi:10.1080/21870764.2020.1847424

Pezzato, L., Rigon, M., Martucci, A., Brunelli, K., and Dabalà, M. (2019). Plasma Electrolytic Oxidation (PEO) as Pre-treatment for Sol-Gel Coating on Aluminum and Magnesium Alloys. *Surf. Coat. Technol.* 366, 114–123. doi:10.1016/j.surfcoat.2019.03.023

Shi, L., Liu, X., Shi, L., Stinson, H. T., Rowlette, J., Kahl, L. J., et al. (2020). Mid-infrared Metabolic Imaging with Vibrational Probes. *Nat. Methods* 17, 844–851. doi:10.1038/s41592-020-0883-z

Toorani, M., Aliofkhazraei, M., Mahdavian, M., and Naderi, R. (2020). Effective PEO/Silane Pretreatment of Epoxy Coating Applied on AZ31B Mg alloy for Corrosion protection. *Corrosion Sci.* 169, 108608. doi:10.1016/j.corsci.2020.108608

Toorani, M., Aliofkhazraei, M., Mahdavian, M., and Naderi, R. (2021). Superior Corrosion protection and Adhesion Strength of Epoxy Coating Applied on AZ31 Magnesium alloy Pre-treated by PEO/Silane with Inorganic and Organic Corrosion Inhibitors. *Corrosion Sci.* 178, 109065. doi:10.1016/j.corsci.2020.109065

Toorani, M., Aliofkhazraei, M., and Naderi, R. (2019). Ceria-embedded MAO Process as Pretreatment for Corrosion protection of Epoxy Films Applied on AZ31-magnesium alloy. *J. Alloys Comp.* 785, 669–683. doi:10.1016/j.jallcom.2018.12.257

Toorani, M., and Aliofkhazraei, M. (2019). Review of Electrochemical Properties of Hybrid Coating Systems on Mg with Plasma Electrolytic Oxidation Process as Pretreatment. *Surf. Inter.* 14, 262–295. doi:10.1016/j.surfin.2019.01.004

Trentin, A., Harb, S. V., Uvida, M. C., Pulcinelli, S. H., Santilli, C. V., Marcoen, K., et al. (2019). Dual Role of Lithium on the Structure and Self-Healing Ability of PMMA-Silica Coatings on AA7075 Alloy. *ACS Appl. Mater. Inter.* 11, 40629–40641. doi:10.1021/acsami.9b13839

Trindade, G. F., Abel, M.-L., Lowe, C., Tshulu, R., and Watts, J. F. (2018). A Time-Of-Flight Secondary Ion Mass Spectrometry/Multivariate Analysis (ToF-SIMS/MVA) Approach to Identify Phase Segregation in Blends of Incompatible but Extremely Similar Resins. *Anal. Chem.* 90, 3936–3941. doi:10.1021/acs.analchem.7b04877

Visser, P., Gonzalez-Garcia, Y., Mol, J. M. C., and Terryn, H. (2018). Mechanism of Passive Layer Formation on AA2024-T3 from Alkaline Lithium Carbonate Solutions in the Presence of Sodium Chloride. *J. Electrochem. Soc.* 165, C60–C70. doi:10.1149/2.1011802jes

Visser, P., Liu, Y., Terryn, H., and Mol, J. M. C. (2016). Lithium Salts as Leachable Corrosion Inhibitors and Potential Replacement for Hexavalent Chromium in Organic Coatings for the protection of Aluminum Alloys. *J. Coat. Technol. Res.* 13413, 557–566. doi:10.1007/s11998-016-9784-6

Visser, P., Marcoen, K., Trindade, G. F., Abel, M.-L., Watts, J. F., Hauffman, T., et al. (2019). The Chemical Throwing Power of Lithium-Based Inhibitors from Organic Coatings on AA2024-T3. *Corrosion Sci.* 150, 194–206. doi:10.1016/j.corsci.2019.02.009

Visser, P., Meeusen, M., Gonzalez-Garcia, Y., Terryn, H., and Mol, J. M. C. (2017). Electrochemical Evaluation of Corrosion Inhibiting Layers Formed in a Defect from Lithium-Leaching Organic Coatings. *J. Electrochem. Soc.* 164, C396–C406. doi:10.1149/2.1411707jes

Visser, P., Terryn, H., and Mol, J. M. C. (2019). Active Corrosion protection of Various Aluminium Alloys by Lithium-leaching Coatings. *Surf. Interf. Anal.* 51, 1276–1287. doi:10.1002/sia.6638

Visser, P., Terryn, H., and Mol, J. M. C. (2018). On the Importance of Irreversibility of Corrosion Inhibitors for Active Coating protection of AA2024-T3. *Corrosion Sci.* 140, 272–285. doi:10.1016/j.corsci.2018.05.037

Wu, D., Ma, L., Liu, B., Zhang, D., Minhas, B., Qian, H., et al. (2021). Long-term Deterioration of Lubricant-Infused Nanoporous Anodic Aluminium Oxide Surface Immersed in NaCl Solution. *J. Mater. Sci. Technol.* 64, 57–65. doi:10.1016/j.jmst.2019.12.008

Wu, D., Zhang, D., Ye, Y., Ma, L., Minhas, B., Liu, B., et al. (2019). Durable Lubricant-Infused Anodic Aluminum Oxide Surfaces with High-Aspect-Ratio Nanochannels. *Chem. Eng. J.* 368, 138–147. doi:10.1016/j.cej.2019.02.163

Yan, Y. M., Maltseva, A., Zhou, P., Li, X. J., Zeng, Z. R., Gharbi, O., et al. (2020). On the *In-Situ* Aqueous Stability of an Mg-Li-(Al-Y-Zr) alloy: Role of Li. *Corros. Sci.* 164, 1–36. doi:10.1016/j.corsci.2019.108342

Yang, J., Blawert, C., Lamaka, S. V., Snihirova, D., Lu, X., Di, S., et al. (2018). Corrosion protection Properties of Inhibitor Containing Hybrid PEO-Epoxy Coating on Magnesium. *Corrosion Sci.* 140, 99–110. doi:10.1016/j.corsci.2018.06.014

Yang, J., Di, S., Blawert, C., Lamaka, S. V., Wang, L., Fu, B., et al. (2018). Enhanced Wear Performance of Hybrid Epoxy-Ceramic Coatings on Magnesium Substrates. *ACS Appl. Mater. Inter.* 10, 30741–30751. doi:10.1021/acsami.8b10612

Yasakau, K. A., Zheludkevich, M. L., Lamaka, S. V., Lamaka, Mario. G. S. Ferreira., and Ferreira, M. G. S. (2006). Mechanism of Corrosion Inhibition of AA2024 by Rare-Earth Compounds. *J. Phys. Chem. B* 110, 5515–5528. doi:10.1021/jp0560664

Zaraska, L., Sulka, G. D., Szeremeta, J., and Jaskuła, M. (2010). Porous Anodic Alumina Formed by Anodization of Aluminum alloy (AA1050) and High Purity Aluminum. *Electrochimica Acta* 55, 4377–4386. doi:10.1016/j.electacta.2009.12.054

Zeng, D., Liu, Z., Bai, S., and Zhao, J. (2021). Preparation and Characterization of a Silane Sealed Peo Coating on Aluminum alloy. *Coatings* 11. doi:10.3390/coatings11050549

Zhang, F., Ju, P., Pan, M., Zhang, D., Huang, Y., Li, G., et al. (2018). Self-healing Mechanisms in Smart Protective Coatings: A Review. *Corrosion Sci.* 144, 74–88. doi:10.1016/j.corsci.2018.08.005

Zhang, G., Wu, L., Serdechnova, M., Tang, A., Wang, C., Blawert, C., et al. (2021). *In-situ* LDHs Growth on PEO Coatings on AZ31 Magnesium alloy for Active protection: Roles of PEO Composition and Conversion Solution. *J. Magnesium Alloys* 11, 1–14. doi:10.1016/j.jma.2021.09.001

Conflict of Interest: The authors declare that the research was conducted in the absence of any commercial or financial relationships that could be construed as a potential conflict of interest.

Publisher's Note: All claims expressed in this article are solely those of the authors and do not necessarily represent those of their affiliated organizations, or those of the publisher, the editors, and the reviewers. Any product that may be evaluated in this article, or claim that may be made by its manufacturer, is not guaranteed or endorsed by the publisher.